applied sciences

Article

Divergence of High-Order Harmonic Generation by a Convex Plasma Surface

Chun Yang [1,2,†], Chuliang Zhou [1,*,†], Yinghui Zheng [1], Dongdong Zhang [1,2], Jixing Gao [1,2], Yafeng Bai [1], Rong Qi [1], Jiayi Qian [1], Jiayan Gui [1], Zongxin Zhang [1], Ye Tian [1,*] and Zhinan Zeng [1,*]

1 State Key Laboratory of High Field Laser Physics, Shanghai Institute of Optics and Fine Mechanics, Chinese Academy of Sciences, Shanghai 201800, China; yangchun@siom.ac.cn (C.Y.); yhzheng@siom.ac.cn (Y.Z.); ddzhang@siom.ac.cn (D.Z.); gaojixing@siom.ac.cn (J.G.); baiyafeng@siom.ac.cn (Y.B.); qirong@siom.ac.cn (R.Q.); qianjiayi@siom.ac.cn (J.Q.); jygui@siom.ac.cn (J.G.); zzx@siom.ac.cn (Z.Z.)
2 Center of Materials Science and Optoelectronics Engineering, University of Chinese Academy of Sciences, Beijing 100049, China
* Correspondence: chuliangzhou@siom.ac.cn (C.Z.); tianye@siom.ac.cn (Y.T.); zhinan_zeng@mail.siom.ac.cn (Z.Z.)
† These authors contributed equally to this work.

Abstract: The electron density profile on a plasma surface has a decisive influence on the mechanism and characteristics of the plasma high-order harmonic generation. When the pre-pulse has a similar spatial and temporal distribution as the main laser pulse, the plasma surface on the target will expand to form a convex profile of the similar size as the focal spot of the main pulse. We experimentally observed that the divergence of the harmonics generated by the relativistic laser light incident on a silica target has a saddle-shaped structure. The two-dimensional particle-in-cell simulation with convex plasma surfaces explains the experimental results very well and infers a $0.12\lambda_L$ plasma scale length around the center of the convex profile. Further, we qualitatively explained that the asymmetry of the saddle-shaped harmonic divergence is caused by oblique incidence.

Keywords: laser-plasma interaction; high-intensity laser; strong field physics; high-order harmonic generation; plasma surface

Citation: Yang, C.; Zhou, C.; Zheng, Y.; Zhang, D.; Gao, J.; Bai, Y.; Qi, R.; Qian, J.; Gui, J.; Zhang, Z.; et al. Divergence of High-Order Harmonic Generation by a Convex Plasma Surface. *Appl. Sci.* **2022**, *12*, 5745. https://doi.org/10.3390/app12115745

Academic Editor: Cristian Focsa

Received: 12 May 2022
Accepted: 5 June 2022
Published: 6 June 2022

1. Introduction

The technique of chirped pulse amplification (CPA) [1] could generate ultra-intense laser pulses with intensities ranging from 10^{14} to 10^{23} Wcm^{-2} in the laboratory [2]. For an intensity greater than 10^{18} Wcm^{-2}, the interaction of laser light with matter is dominated by the relativistic character of the electrons. With the increase in laser intensity, the interaction of the laser with over-dense plasma to generate high-order harmonics [3] efficiently has attracted increasing research interests, such as the attosecond lighthouse [4,5], laser-plasma electron acceleration [6], and X-ray nonlinear optics [7]. In the future, relativistic laser and plasma surface interaction is a hopeful route to achieving quantum electrodynamic critical fields [8,9] and zeta-second pulses [10].

High-order harmonic generation (HHG) is an important route to a bright coherent XUV/X-ray source, which has been investigated in many media, such as gases [11,12], clusters [13] and laser-irradiated plasma surfaces [14–16]. The harmonic generation of gas needs to avoid strong ionization of the gaseous medium, so the laser intensity is usually limited below 10^{16} Wcm^{-2}. In contrast, HHG from plasma surfaces has no laser intensity limitation and has significantly higher conversion efficiency for high photon energy sources, e.g., X-rays. In experiments, due to the ablation of the target caused by the pre-pulse, the plasma surface will inevitably expand into the vacuum, forming a density gradient profile called pre-plasma. If this density profile can be expressed as $n(x)$, where x is the spatial coordinate, $L = n(x)/|\nabla n(x)|$ is the plasma scale length.

The electron density gradient scale length of the pre-plasma has a decisive influence on the HHG. For interactions between the laser field and the plasma with a sharp density profile $L < 0.02\lambda_L$, where λ_L is the wavelength of driving pulses, the electrons on the plasma surface are first pulled out of the plasma by the laser field, and then pushed back into the dense plasma by the reversed laser field. These electrons, called vacuum-accelerated Brunel electrons [17,18], carry away energy into dense plasma and generate harmonics named coherent wake emission (CWE) [19,20]. For a relativistic intensity laser interacting with a long density gradient of L less than $0.2\lambda_L$, the incident laser field is reflected around the critical surface, where the electrons behave as relativistic oscillations. The HHG is attributed to a periodic Doppler effect induced by the relativistic oscillations of the electrons, called a relativistic oscillating mirror (ROM) [10,21,22]. As for a plasma scale length L larger than $0.2\lambda_L$, an excessively long pre-plasma will induce parametric instability and greatly reduce the coherence of the harmonics [23]. The optimal scale length of pre-plasma to generate harmonics exists within a range [24] from 0 to $0.2\lambda_L$, where the mechanism of harmonic generation transitions from CWE to ROM [25]. For example, a laser with a high contrast ratio will form a sharp pre-plasma, and the plasma scale length L will exceed a threshold only at the center of the laser spot, resulting in an annular CWE source [26]. A curved plasma surface created by laser radiation pressure can focus the harmonics [27–29], which means a shaped plasma surface can be used to control the harmonic divergence [30].

In this letter, we report the HHG driven by a 12.6J 800 nm laser pulse at the laser peak intensity of $I_0 = 1.6 \times 10^{20}$ Wcm^{-2}. We find an asymmetric saddle-shaped structure of the harmonic divergence, which can be explained by the harmonics reflected from a Gaussian convex plasma surface formed by a Gaussian pre-pulse with a similar spatial distribution as the main pulse. This is confirmed by 2D particle-in-cell (PIC) simulations, deducing a density scale length of $\sim 0.12\lambda_L$ at the center of the plasma surface. Further analysis shows that the asymmetry of harmonic divergence is caused by an oblique incidence of the laser on the convex plasma surface. Our study provides insights into the divergence control of harmonics from plasma surfaces.

2. Experimental Results

The experiments of plasma harmonics are performed on the 1 PW/0.1 Hz laser system of the Shanghai Superintense Ultrafast Laser Facility (SULF) [31].The experimental system mainly consists of a laser, vacuum chamber and home-made flat field grating spectrometer. The SULF facility can deliver a 29.6 fs (full width at half maximum, FWHM) laser pulse with a diameter of 200 mm and central wavelength at 800 nm, and the single pulse on-target energy used in experiments can be up to 12.6J. This experiment was performed before mounting the plasma mirror. The contrast ratio at 80 picoseconds before the main pulse (−80 ps) is about 2.5×10^{-11}, but the contrast ratio at −10 picoseconds is only about 1×10^{-5}.

The schematic diagram in the vacuum chamber is shown in Figure 1a. Through a $f/3$ off-axis parabolic mirror (OAP, f = 600 mm, off-axis angle = 26°) , the laser pulse was focused on the polished fused silica plates, whose electron density is $n_{max} \simeq 400n_c$ when entirely ionized, where n_c is the critical density for the incident wave. The focal spot size was 6.0 µm (FWHM), corresponding to a peak intensity of $I_0 = 1.6 \times 10^{20}$ Wcm^{-2} (normalized vector potential $a_0 = \sqrt{I_0\lambda_L^2/(1.38 \times 10^{18}\ \mathrm{Wcm^{-2}\mu m^2})} \simeq 8$) on target. The radiation generated from such geometry was measured with a home-made flat-field grating spectrometer. In the reflection direction, the high-order harmonics passed through a 2 mm wide slit and a 250 nm-thick aluminum (Al) foil filter. The flat field grazing-incidence grating (Hitachi, 1200 lines/mm) was 237 mm away from the slit, and the soft X-ray CCD (Andor, DO940P-BEN) was located at the focal plane of the grating. The horizontal direction in the CCD array represents the wavelength coordinate, which was calibrated by the L3 absorption edge (17.1 nm) of aluminum. Due to the limitation of the experimental layout, the angle between the observation direction of the spectrometer and the incident laser was fixed at 116 degrees. Figure 1b represents the harmonic signal from vertically integral of CCD image.

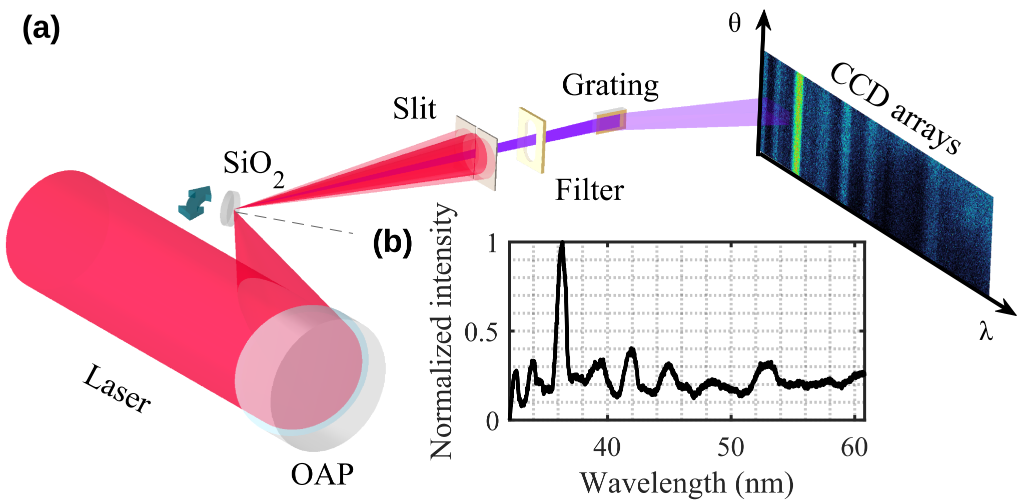

Figure 1. Measurement of spatial distribution of high-order harmonic generation. (**a**) Experimental setup. The angle between the observation direction of the spectrometer and the incident laser was 116°. We rotated the plasma surface to observe the divergence of high-order harmonic generation. The horizontal direction in the CCD array represents the wavelength coordinate. (**b**) Vertically integral of CCD image. The L3 absorption edge of aluminum calibrated the spectra.

In order to observe the divergence of HHG, we adjusted the incident angle by fixing the incident laser and rotating the plasma surface. In general, the so-called divergence of harmonics should be measured by fixing the incident angle of pulses and then adjusting the receiving angle of the detector. This is difficult to achieve experimentally and why we rotated the plasma surface to measure the divergence. It can be seen from Figure 1a that the reflected beam rotated by 2 degrees when the target plane rotated by 1 degree. On the horizontal plane, we rotated the target plane so that the incident angle of the main pulse changed from 42 degrees to 70 degrees. The spectra captured by the CCD arrays indicated that the high-order harmonic signal can be observed in a range of about ∼56°. Further, we found that the observed HHG signal depends on the angle of incidence, as shown in Figure 2. Unlike the Gaussian type of incident light, the distribution of HHG intensity with an incident angle exhibits a saddle-shaped structure, which we will discuss in the following sections.

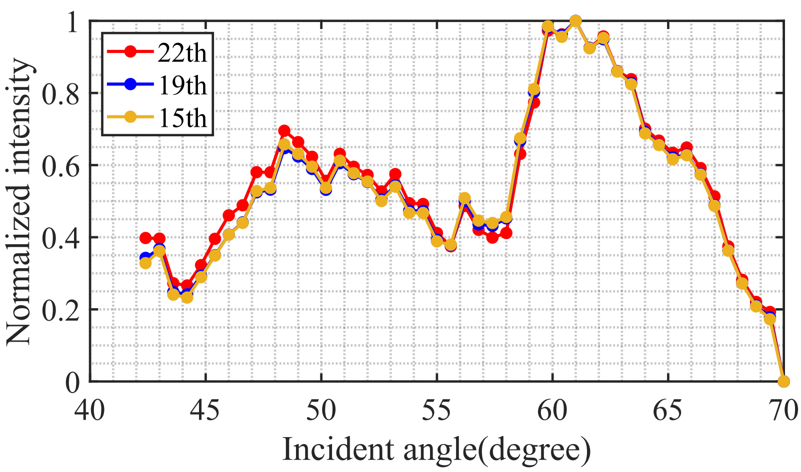

Figure 2. The intensity of high-order harmonics at different incident angles. Different from an incident beam, there are two peaks in the angular distribution, and the peak at 61° is slightly higher than the one at 48°.

3. Simulation and Discussion

From a geometrical optics point of view, the divergence of light reflected from a flat plasma surface is usually similar to that of the incident laser, as observed in many experiments [20,32]. If a Gaussian incident laser beam is focused onto a plasma surface, the resulting harmonics are also usually Gaussian. In our experiments, the difference in the divergence of the harmonics and incident laser implies the information of the plasma surface. We, therefore, assume that a non-Gaussian harmonic divergence is generated from the uneven plasma surface due to the pre-pulse. Disregarding the energy (ϵ_e) of the electron oscillating in the magnetic field, the energy of the electrons on the plasma surface oscillating in the electric field of the incident laser is [33]

$$\epsilon_e(r) = [\gamma(\mathrm{r}) - 1]m_e c^2, \gamma(\mathrm{r}) = \left[1 + a_0^2(\mathrm{r})\right]^{1/2} \tag{1}$$

where r is a coordinate along the plasma surface, m_e is the electron mass and c is the velocity of light. For $a_0 \ll 1$, $\epsilon_e \propto a_0^2$; and for $a_0 \gg 1$, $\epsilon_e \propto a_0$. Therefore, after the Gaussian beam reaches the plasma surface, the spatial distribution of the thermal electron expansion velocity on the plasma surface can be approximated as a Gaussian distribution. In brief, after the action of the pre-pulse, the plasma surface in the center of the focal spot has a larger expansion speed, which induces a larger plasma scale length L. In this case, the pre-pulse acting on the plasma surface is assumed to induce a convex plasma surface profile. When the main pulse is incident on this convex plasma surface, the harmonics emissions will exhibit divergence characteristics different from the flat plasma surface.

To verify our hypothesis and support our experimental results, we compared the high-order harmonic spectrum generated by the relativistic laser incident on different shaped plasma surfaces by means of 2D PIC simulation with EPOCH code [34]. The parameters of laser and electron density are similar to our experimental conditions. In the x-y plane, the p-polarized light with a relativistic light intensity of $a_0 = 8$ is incident from the y+ boundary, the wavelength is λ_L = 800 nm, the pulse width is $3T_0$ (FWHM, T_0 is laser period), and the beam waist size of the Gaussian beam is $4\lambda_L$ (FWHM). The maximum density of the plasma electrons is calculated from the parameters of silica (mass density ρ = 2.65 g/cm^3, relative molecular mass M_r = 60.0830 g/mol) (assuming that the electrons are fully ionized), and the peak density is about $400n_c$. Due to the presence of the pre-pulse, the plasma surface of the target has an electron density distribution of an exponential gradient profile $n_e(r_\parallel, r_\perp) = n_{max}\exp\left[-r_\perp/L\left(r_\parallel\right)\right]$, where $(r_\parallel, r_\perp)$ are the coordinates parallel and perpendicular to the plasma surface, respectively, and $L\left(r_\parallel\right)$ is the plasma scale length at $r_\parallel$. The distribution of the Gaussian plasma scale length can be given as $L\left(r_\parallel\right) = L_0\exp\left[-4\ln 2(r_\parallel/w_0)^2\right]$, where $w_0 = 4\lambda_L$ (FWHM) is the same as the focal spot of the incident laser, and L_0 is the plasma scale length at $r_\parallel = 0$. Therefore, the electron density of convex plasma surface used in simulations could be expressed as

$$n_e\left(r_\parallel, r_\perp\right) = n_{\max}\exp\left\{-\frac{r_\perp}{L_0\exp\left[-4\ln 2\left(r_\parallel/w_0\right)^2\right]}\right\} \tag{2}$$

For comparison, we also simulated the case of a flat pre-plasma surface, in this case $L\left(r_\parallel\right) = 0.06\lambda_L$. To be consistent with the experimental setup, in our simulations, instead of changing the beam incidence direction, we changed the angle of incidence by rotating the plasma surface so that the change in the angle of incidence was in the range of 40∼70 degrees. The size of the calculation space is $20\lambda_L \times 30\lambda_L$, the space step size is $\Delta x = \Delta y = 0.005\lambda_L$, the time step is $0.0033T_0$, and there are about 58 virtual particles in each cell.

The simulation results of convex and flat plasma surfaces are shown in Figure 3a,c, respectively, where the incident angle is 45 degrees, $t = 24T_0$. The plasma is represented by a grey color bar, the pre-plasma is located on the upper surface, and the thickness of the plasma is $3\lambda_L$, which is sufficient to reflect high-order harmonics. The light field is represented by a red and blue color bar, the red arrow represents the direction of the driving laser, the focal point of the driving laser is at (0, 0), and the gray arrow represents the propagation direction of the reflected wave. From Figure 3a, we can see that the wavefront of the reflected wave generated by the convex plasma surface is clearly divided into two peaks, while for the flat target of Figure 3b, there is only one peak. The difference in the reflected wavefront is caused by the difference in the distribution of the pre-plasma. To support our experimental results, we set the output of the reflected light field at an angle of 116 degrees to the incident light to obtain the harmonic spectrum. Identical to the experimental setup, we varied the incident angle by rotating the plasma surface around the laser focus, ranging from 40∼70 degrees. Figure 3b shows the 5th–50th harmonic spectrum reflected by the convex plasma surface at different incident angles. It can be seen from the figure that there are harmonic peaks at the 50° and 60° directions (white dashed lines, labeled peak A and peak B, respectively). In contrast, the flat target reflected harmonics with only one peak, as shown by the dashed line in Figure 3d. It can be seen from the simulation that the assumption of convex plasma is in good agreement with the experiment.

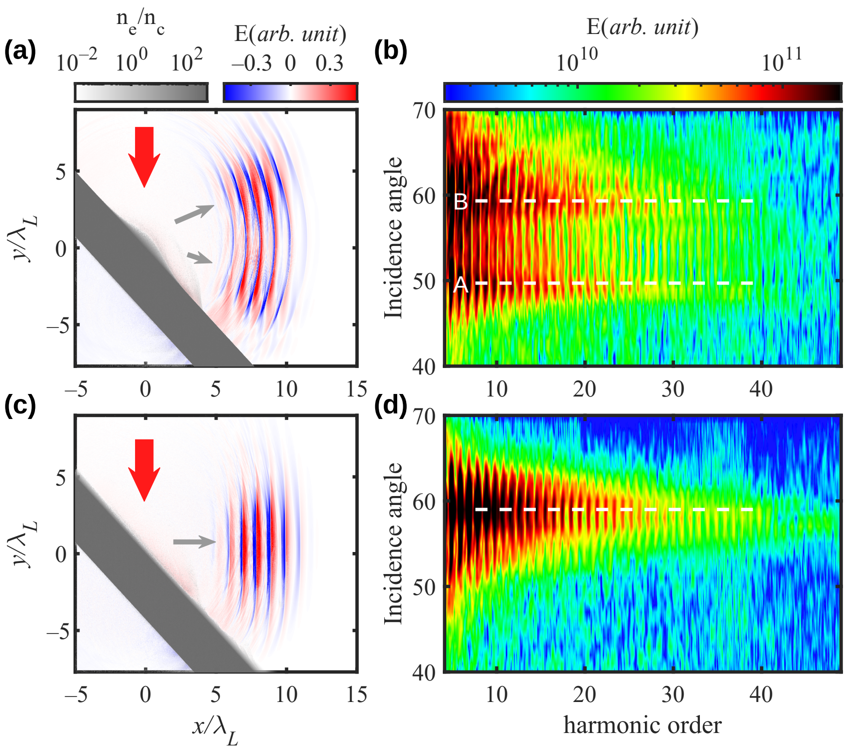

Figure 3. Simulated images of the convex (**a**) and the flat (**c**) plasma surface at time $t = 24T_0$. (**a**) The driving laser (red arrow) with relativistic intensity $a_0 = 8$ is incident on the convex plasma surface at an incident angle of 45 degrees, and the wavefront of the reflected wave mainly has two peaks (grey arrow). (**c**) The simulation setup is the same as (**a**), except for the flat plasma surface, where one can see a peak in the reflected wavefront. The harmonic spectrum was observed at an angle of 116 degrees to the incident light. By rotating the plasma surface, harmonic spectra of reflections from a convex (**b**) and a flat (**d**) plasma surface were observed.

In the divergent spectrum of the harmonics observed in our experiments, the intensity of the peak at 60 degrees is always greater than that at 50 degrees, which can be interpreted from the distribution of electrons on the plasma surface. Due to the electron heating caused by the pre-pulse, the thermal motion of the electrons manifests as an expansion perpendicular to the plasma surface, forming a pre-plasma, as shown in Figure 4a. For the plasma target of $n_{max} = 400n_c$, the distance from the reflection surface of the fundamental frequency light ($n_e = n_c$) to the initial plasma surface is $\delta = L\left(r_{\parallel}\right) \times \ln(n_{\max}/n_c)$. We assume that the scale length at $r_{\parallel} = 0$ is $L\left(r_{\parallel} = 0\right) = 0.12\lambda_L$, so $\delta\left(r_{\parallel} = 0\right) \cong 0.72\lambda_L$. Due to oblique incidence, the central reflection point is laterally offset relative to the main pulse by a distance $\delta \sin\theta$. As a result, the main pulse energy is unevenly distributed on both sides of the reflection axis, as indicated by peaks A (violet) and B (red) in Figure 4a, and the intensity of peak B is always greater than that of peak A. This is confirmed in both our experiments and simulations. Figure 4b shows the intensity of the 22nd harmonic at different incident angles, and the peaks of its spectra divergence are located at 51 degrees (A) and 60 degrees (B), respectively. The intensity of peak A is about 80 percent of peak B, which is close to 70 percent of the experimental results. Correspondingly, the divergence of the 22nd harmonic reflected by the flat plasma surface presents a Gaussian structure. Our simulations reproduce well the phenomena observed in the experiments.

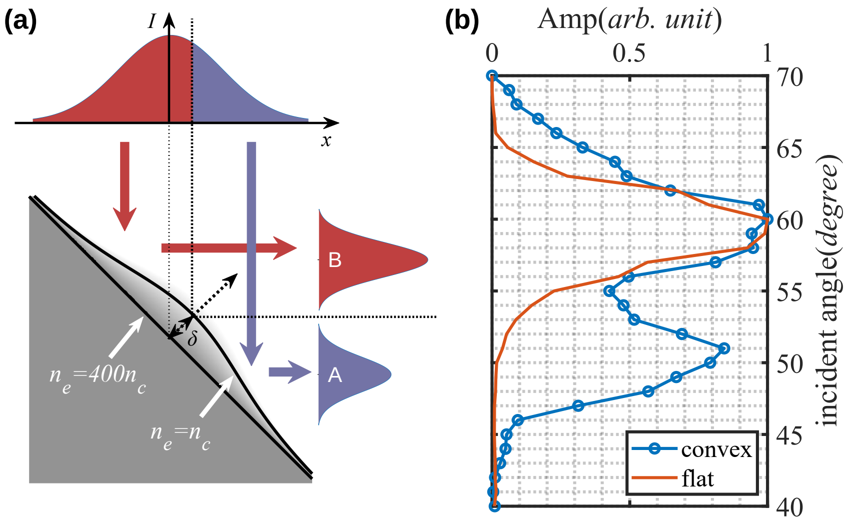

Figure 4. (**a**) Schematic diagram of a relativistic laser incident on a convex plasma surface. Due to the plasma expansion, the $n_e = n_c$ interface is shifted by a distance δ in the direction perpendicular to the target, which causes the reflection center to be shifted by $\delta \sin\theta$ relative to the main pulse. Therefore, the Gaussian main pulse is divided into two parts, A and B, after reflection, where A has less energy than B. (**b**) The intensity of the 22nd harmonic generated by the convex (blue) and flat (red) plasma surface at different incident angles.

4. Conclusions

To conclude, we report high-order harmonic generation on a plasma surface with the relativistic light of intensity $a_0 = 8$. The results show that the high-order harmonic divergence has a saddle-shaped structure. Further analysis shows that a Gaussian gradient distribution formed on the plasma surface before the arrival of the main pulse can lead to this saddle-shaped structure of divergence on the harmonic spectrum. We compared the divergence of harmonics generated by a relativistic laser incident on plasma surfaces with different shapes using PIC simulations and confirmed that the divergence of harmonics from a Gaussian gradient plasma surface coincides very well with experiments. Our work shows that the shape of the plasma surface has a very important effect on the generation of high-order harmonics, which provides useful insights into the generation and application [27–29,35] of higher brightness high-order harmonics and the tools to control the emission of high-order harmonics in the future, e.g., natural focused harmonics.

Author Contributions: Conceptualization, writing—original draft preparation, C.Y.; data curation and visualization, C.Y. and C.Z.; methodology, writing—review and editing, C.Y., C.Z., Y.T. and Z.Z. (Zhinan Zeng); investigation, C.Z., Y.Z., D.Z., J.G. (Jixing Gao), Y.B., R.Q., J.Q., J.G. (Jiayan Gui) and Z.Z. (Zongxin Zhang); supervision, project administration and funding acquisition, C.Z., Y.T. and Z.Z. (Zhinan Zeng). All authors have read and agreed to the published version of the manuscript.

Funding: This work has received funding from the National Natural Science Foundation of China (grants Nos. 91950203, 11922412, 11874372, 11874374), Shanghai Pilot Program for Basic Research—Chinese Academy of Science, Shanghai Branch, Key Research Program of Frontier Sciences, Chinese Academy of Science and Youth Innovation Promotion Association of Chinese Academy of Sciences, as well as funding from Young Talents Support Project of China Association for Science and Technology, China Postdoctoral Science Foundation (grant No. 2021M703329), Shanghai Sailing Program under Grant 22YF1455000. PIC simulations were run using EPOCH codes, which was in part funded by the UK EPSRC grants EP/G054950/1, EP/G056803/1, EP/G055165/1 and EP/ M022463/1.

Institutional Review Board Statement: Not applicable.

Informed Consent Statement: Not applicable.

Data Availability Statement: The data supporting the findings of this study are available from the corresponding author upon reasonable request.

Acknowledgments: The authors acknowledge Shanghai Supercomputer Center for providing computing resources.

Conflicts of Interest: The authors declare no conflict of interest.

References

1. Strickland, D.; Mourou, G. Compression of amplified chirped optical pulses. *Opt. Commun.* **1985**, *56*, 219–221. [CrossRef]
2. Yoon, J.W.; Kim, Y.G.; Choi, I.W.; Sung, J.H.; Lee, H.W.; Lee, S.K.; Nam, C.H. Realization of laser intensity over 1e23 W/cm^2. *Optica* **2021**, *8*, 630. [CrossRef]
3. Baeva, T.; Gordienko, S.; Pukhov, A. Theory of high-order harmonic generation in relativistic laser interaction with overdense plasma. *Phys. Rev. E* **2006**, *74*, 046404. [CrossRef] [PubMed]
4. Wheeler, J.A.; Borot, A.; Monchocé, S.; Vincenti, H.; Ricci, A.; Malvache, A.; Lopez-Martens, R.; Quéré, F. Attosecond lighthouses from plasma mirrors. *Nat. Photonics* **2012**, *6*, 829–833. [CrossRef]
5. Vincenti, H.; Quere, F. Attosecond Lighthouses: How to Use Spatiotemporally Coupled Light Fields to Generate Isolated Attosecond Pulses. *Phys. Rev. Lett.* **2012**, *108*, 113904. [CrossRef]
6. Corde, S.; Ta Phuoc, K.; Lambert, G.; Fitour, R.; Malka, V.; Rousse, A.; Beck, A.; Lefebvre, E. Femtosecond X-rays from laser-plasma accelerators. *Rev. Mod. Phys.* **2013**, *85*, 1–48. [CrossRef]
7. Martín, L.; Benlliure, J.; Cortina-Gil, D.; Peñas, J.; Ruiz, C. Improved stability of a compact vacuum-free laser-plasma X-ray source. *High Power Laser Sci. Eng.* **2020**, *8*, 6948110. [CrossRef]
8. Bulanov, S.V.; Esirkepov, T.; Tajima, T. Light intensification towards the Schwinger limit. *Phys. Rev. Lett.* **2003**, *91*, 085001. [CrossRef] [PubMed]
9. Ribeyre, X.; d'Humieres, E.; Jansen, O.; Jequier, S.; Tikhonchuk, V.T.; Lobet, M. Pair creation in collision of gamma-ray beams produced with high-intensity lasers. *Phys. Rev. E* **2016**, *93*, 013201. [CrossRef]
10. Gordienko, S.; Pukhov, A.; Shorokhov, O.; Baeva, T. Relativistic Doppler effect: Universal spectra and zeptosecond pulses. *Phys. Rev. Lett.* **2004**, *93*, 115002. [CrossRef] [PubMed]
11. L'Huillier, A.; Balcou, P. High-order harmonic generation in rare gases with a 1-ps 1053-nm laser. *Phys. Rev. Lett.* **1993**, *70*, 774–777. [CrossRef] [PubMed]
12. Krause, J.L.; Schafer, K.J.; Kulander, K.C. High-order harmonic generation from atoms and ions in the high intensity regime. *Phys. Rev. Lett.* **1992**, *68*, 3535–3538. [CrossRef]
13. Wabnitz, H.; Bittner, L.; de Castro, A.R.; Dohrmann, R.; Gurtler, P.; Laarmann, T.; Laasch, W.; Schulz, J.; Swiderski, A.; von Haeften, K.; et al. Multiple ionization of atom clusters by intense soft X-rays from a free-electron laser. *Nature* **2002**, *420*, 482–485. [CrossRef] [PubMed]
14. Zhang, J.; Zepf, M.; Norreys, P.A.; Dangor, A.E.; Bakarezos, M.; Danson, C.N.; Dyson, A.; Fews, A.P.; Gibbon, P.; Key, M.H.; et al. Coherence and bandwidth measurements of harmonics generated from solid surfaces irradiated by intense picosecond laser pulses. *Phys. Rev. A* **1996**, *54*, 1597–1603. [CrossRef]
15. Teubner, U.; Gibbon, P. High-order harmonics from laser-irradiated plasma surfaces. *Rev. Mod. Phys.* **2009**, *81*, 445–479. [CrossRef]
16. Gibbon, P. Harmonic generation by femtosecond laser-solid interaction: A coherent "water-window" light source? *Phys. Rev. Lett.* **1996**, *76*, 50–53. [CrossRef] [PubMed]
17. Brunel, F. Not-so-resonant, resonant absorption. *Phys. Rev. Lett.* **1987**, *59*, 52–55. [CrossRef]

18. Thaury, C.; Quere, F. High-order harmonic and attosecond pulse generation on plasma mirrors: Basic mechanisms. *J. Phys. B-At. Mol. Opt. Phys.* **2010**, *43*, 213001. [CrossRef]
19. Quere, F.; Thaury, C.; Monot, P.; Dobosz, S.; Martin, P.; Geindre, J.P.; Audebert, P. Coherent wake emission of high-order harmonics from overdense plasmas. *Phys. Rev. Lett.* **2006**, *96*, 125004. [CrossRef]
20. Thaury, C.; Quéré, F.; Geindre, J.P.; Levy, A.; Ceccotti, T.; Monot, P.; Bougeard, M.; Réau, F.; d'Oliveira, P.; Audebert, P.; et al. Plasma mirrors for ultrahigh-intensity optics. *Nat. Phys.* **2007**, *3*, 424–429. [CrossRef]
21. Lichters, R.; Meyer-ter-Vehn, J.; Pukhov, A. Short-pulse laser harmonics from oscillating plasma surfaces driven at relativistic intensity. *Phys. Plasmas* **1996**, *3*, 3425–3437. [CrossRef]
22. Tsakiris, G.D.; Eidmann, K.; Meyer-ter Vehn, J.; Krausz, F. Route to intense single attosecond pulses. *New J. Phys.* **2006**, *8*, 19. [CrossRef]
23. Dollar, F.; Cummings, P.; Chvykov, V.; Willingale, L.; Vargas, M.; Yanovsky, V.; Zulick, C.; Maksimchuk, A.; Thomas, A.G.; Krushelnick, K. Scaling high-order harmonic generation from laser-solid interactions to ultrahigh intensity. *Phys. Rev. Lett.* **2013**, *110*, 175002. [CrossRef] [PubMed]
24. Rodel, C.; an der Brugge, D.; Bierbach, J.; Yeung, M.; Hahn, T.; Dromey, B.; Herzer, S.; Fuchs, S.; Pour, A.G.; Eckner, E.; et al. Harmonic Generation from Relativistic Plasma Surfaces in Ultrasteep Plasma Density Gradients. *Phys. Rev. Lett.* **2012**, *109*, 125002. [CrossRef] [PubMed]
25. Tarasevitch, A.; Lobov, K.; Wunsche, C.; von der Linde, D. Transition to the relativistic regime in high order harmonic generation. *Phys. Rev. Lett.* **2007**, *98*, 103902. [CrossRef]
26. Yehuda, H.; Porat, E.; Cohen, I.; Levi, R.H.; Levanon, A.; Pomerantz, I. Annular coherent wake emission. *Opt. Lett.* **2021**, *46*, 4674–4677. [CrossRef]
27. Vincenti, H.; Monchoce, S.; Kahaly, S.; Bonnaud, G.; Martin, P.; Quere, F. Optical properties of relativistic plasma mirrors. *Nat. Commun.* **2014**, *5*, 3403. [CrossRef]
28. Vincenti, H. Achieving Extreme Light Intensities using Optically Curved Relativistic Plasma Mirrors. *Phys. Rev. Lett.* **2019**, *123*, 105001. [CrossRef] [PubMed]
29. Quéré, F.; Vincenti, H. Reflecting petawatt lasers off relativistic plasma mirrors: A realistic path to the Schwinger limit. *High Power Laser Sci. Eng.* **2021**, *9*, E6. [CrossRef]
30. Gao, J.; Li, B.; Liu, F.; Chen, Z.Y.; Chen, M.; Ge, X.; Yuan, X.; Chen, L.; Sheng, Z.; Zhang, J. Divergence control of relativistic harmonics by an optically shaped plasma surface. *Phys. Rev. E* **2020**, *101*, 033202. [CrossRef] [PubMed]
31. Zhang, Z.; Wu, F.; Hu, J.; Yang, X.; Gui, J.; Ji, P.; Liu, X.; Wang, C.; Liu, Y.; Lu, X.; et al. The 1 PW/0.1 Hz laser beamline in SULF facility. *High Power Laser Sci. Eng.* **2020**, *8*, 1–7. [CrossRef]
32. Kahaly, S.; Monchoce, S.; Vincenti, H.; Dzelzainis, T.; Dromey, B.; Zepf, M.; Martin, P.; Quere, F. Direct Observation of Density-Gradient Effects in Harmonic Generation from Plasma Mirrors. *Phys. Rev. Lett.* **2013**, *110*, 175001. [CrossRef]
33. Wilks, S.C.; Kruer, W.L.; Tabak, M.; Langdon, A.B. Absorption of ultra-intense laser pulses. *Phys. Rev. Lett.* **1992**, *69*, 1383–1386. [CrossRef]
34. Arber, T.D.; Bennett, K.; Brady, C.S.; Lawrence-Douglas, A.; Ramsay, M.G.; Sircombe, N.J.; Gillies, P.; Evans, R.G.; Schmitz, H.; Bell, A.R.; et al. Contemporary particle-in-cell approach to laser-plasma modelling. *Plasma Phys. Control. Fusion* **2015**, *57*, 1–13001. [CrossRef]
35. Zhou, C.; Tian, Y.; Zeng, Y.; Zeng, Z.; Li, R.; Ramakrishna, B. Bright High-Harmonic Generation through Coherent Synchrotron Emission Based on the Polarization Gating Scheme. *Laser Part. Beams* **2022**, *2022*, 6948110. [CrossRef]